Apoastron Shift Constraints

According to GR, the motion of a test particle can be fully described by solving the geodesic equations. Under the assumption that the matter distribution is static and pressureless, the equations of motion at the first post-Newtonian (PN) approximation become (see e.g. (Fock 1961, Weinberg 1972, Rubilar & Eckart 2001))

$$\frac{d\mathbf{v}}{dt} \simeq -\nabla(\Phi_N + 2\Phi_N^2) + 4\mathbf{v}(\mathbf{v}\cdot\nabla)\Phi_N - v^2\nabla\Phi_N \ . \qquad (21)$$

We note that the PN-approximation is the first relativistic correction from which the apoastron advance phenomenon arises. In the case of the S2 star, the apoastron shift as seen from Earth (from Eq. (23)) due to the presence of a central black hole is about 1 mas, therefore not directly

detectable at present since the available precision in the apoastron shift is about 10 mas (but it will become about 1 mas in 10–15 years even without considering possible technological improvements). It is also evident that higher order relativistic corrections to the S2 apoastron shift are even smaller and therefore may be neglected at present, although they may become important in the future.

As it will be discussed below, the Newtonian effect due to the existence of a sufficiently extended DM sphere around the black hole may cause a apoastron shift in the opposite direction with respect to the relativistic advance due to the black hole. Therefore, we have considered the two effects comparing only the leading terms.

For the DM distribution at the Galactic Center we follow Eq. (19) as done in Hall & Gondolo (2006). Clearly, if in the future faint infrared stars (or spots) closer to the black hole with respect to the S2 star will be monitored (Eisenhauer, (2005)), this simplified model might well not hold

and higher order relativistic corrections may become necessary.

For a spherically symmetric mass distribution (such as that described above) and for a gravitational potential given by Eq. (20), Eq. (21) may be rewritten in the form (see for details Rubilar & Eckart (2001))

$$\frac{d\mathbf{v}}{dt} \simeq -\frac{GM(r)}{r^3}\left[\left(1+\frac{4\Phi_N}{c^2}+\frac{v^2}{c^2}\right)\mathbf{r}-\frac{4\mathbf{v}(\mathbf{v}\cdot\mathbf{r})}{c^2}\right] , \qquad (22)$$

r and **v** being the vector radius of the test particle with respect to the center of the stellar cluster and the velocity vector, respectively. Once the initial conditions for the star distance and velocity are given, the rosetta shaped orbit followed by a test particle can be found by numerically solving the set of ordinary differential equations in eq. (22).

In Fig. 20, as an example, assuming that the test particle orbiting the Galactic Center region is the S2 star, we show the Post Newtonian orbits

detectable at present since the available precision in the apoastron shift is about 10 mas (but it will become about 1 mas in 10–15 years even without considering possible technological improvements). It is also evident that higher order relativistic corrections to the S2 apoastron shift are even smaller and therefore may be neglected at present, although they may become important in the future.

As it will be discussed below, the Newtonian effect due to the existence of a sufficiently extended DM sphere around the black hole may cause a apoastron shift in the opposite direction with respect to the relativistic advance due to the black hole. Therefore, we have considered the two effects comparing only the leading terms.

For the DM distribution at the Galactic Center we follow Eq. (19) as done in Hall & Gondolo (2006). Clearly, if in the future faint infrared stars (or spots) closer to the black hole with respect to the S2 star will be monitored (Eisenhauer, (2005)), this simplified model might well not hold

and higher order relativistic corrections may become necessary.

For a spherically symmetric mass distribution (such as that described above) and for a gravitational potential given by Eq. (20), Eq. (21) may be rewritten in the form (see for details Rubilar & Eckart (2001))

$$\frac{d\mathbf{v}}{dt} \simeq -\frac{GM(r)}{r^3}\left[\left(1+\frac{4\Phi_N}{c^2}+\frac{v^2}{c^2}\right)\mathbf{r}-\frac{4\mathbf{v}(\mathbf{v}\cdot\mathbf{r})}{c^2}\right] , \qquad (22)$$

r and **v** being the vector radius of the test particle with respect to the center of the stellar cluster and the velocity vector, respectively. Once the initial conditions for the star distance and velocity are given, the rosetta shaped orbit followed by a test particle can be found by numerically solving the set of ordinary differential equations in eq. (22).

In Fig. 20, as an example, assuming that the test particle orbiting the Galactic Center region is the S2 star, we show the Post Newtonian orbits

obtained by the black hole only, the black hole plus the stellar cluster and the contribution of two different DM mass density profiles. In each case the S2 orbit apoastron shift is given. As one can see, for selected parameters for DM and stellar cluster masses and radii the effect of the stellar cluster is almost negligible while the effect of the DM distribution is crucial since it enormously overcome the shift due to the relativistic precession. Moreover, as expected, its contribution is opposite in sign with respect to that of the black hole (Nucita et al. (2007)).

We note that the expected apoastron (or, equivalently, periastron) shifts (mas/revolution), $\Delta\Phi$ (as seen from the center) and the corresponding values $\Delta\phi_E^{\pm}$ as seen from Earth (at the distance $R_0 \simeq 8$ kpc from the GC) are related by

$$\Delta\phi_E^{\pm} = \frac{d(1 \pm e)}{R_0}\Delta\Phi, \tag{23}$$

where with the sign $\pm$ are indicated the shift angles of the apoastron $(+)$

and periastron (-), respectively. The S2 star semi-major axis and eccentricity are $d = 919$ AU and $e = 0.87$ (Ghez et al. 2005).

In Fig. 32, the S2 apoastron shift as a function of the DM distribution size R_{DM} is given for $\alpha = 0$ and $M_{DM} \simeq 2 \times 10^5$ $M_\odot$. Taking into account that the present day precision for the apoastron shift measurements is of about 10 mas, one can say that the S2 apoastron shift cannot be larger than 10 mas. Therefore, any DM configuration that gives a total S2 apoastron shift larger than 10 mas (in the opposite direction due to the DM sphere) is excluded. The same analysis is shown in Figs. 33 and 34 for two different values of the DM mass distribution slope, i.e. $\alpha = 1$ and $\alpha = 2$, respectively. In any case, we have calculated the apoastron shift for the S2 star orbit assuming a total DM mass $M_{DM} \simeq 2 \times 10^5$ $M_\odot$. As one can see by inspecting Figs. 32-34, the upper limit of about 10 mas on the S2 apoastron shift may allow to conclude that DM radii in the range about $10^{-3} - 10^{-2}$ pc are excluded by present observations.

We notice that the results of the present analysis allows to further constrain the results (Hall and Gondolo 2006) who have concluded that if the DM sphere radius is in the range $10^{-3} - 1$ pc, configurations with DM mass up to $M_{DM} = 2 \times 10^5\ M_\odot$ are acceptable. The present analysis shows that DM configurations of the same mass are acceptable only for R_{DM} out the range between $10^{-3} - 10^{-2}$ pc, almost irrespectively of the α value.

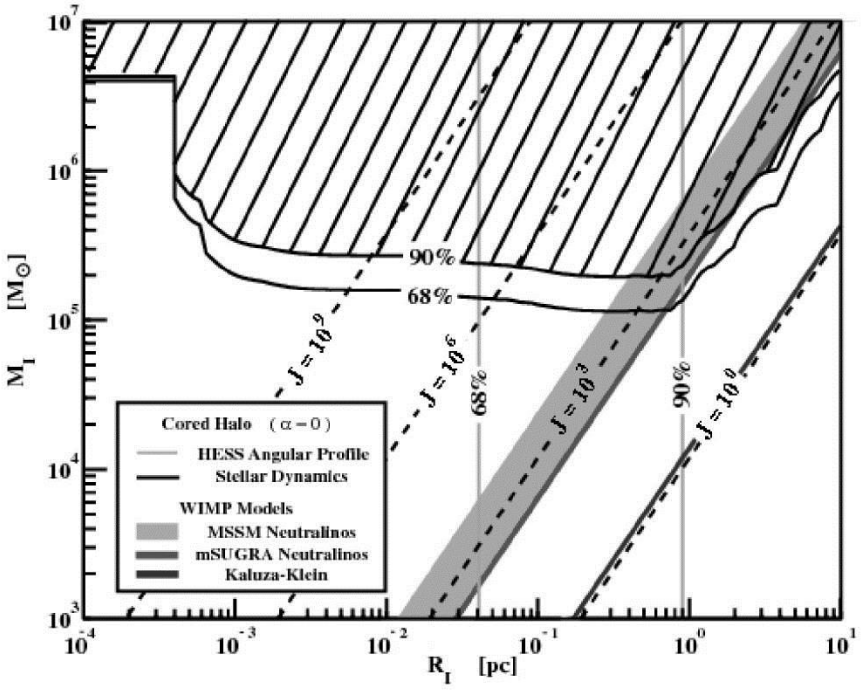

Figure 28: An allowed region for DM distribution from S2 like star trajectories near the Black Hole at the Galactic Center (Hall and Gondolo (2006)).

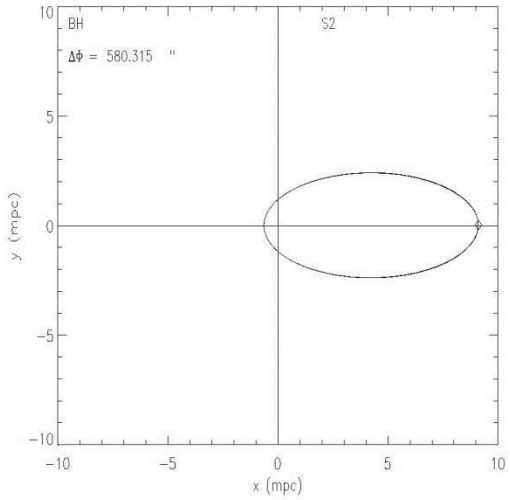
BH
S2
Δϕ = 580.315 "
y (mpc)
x (mpc)

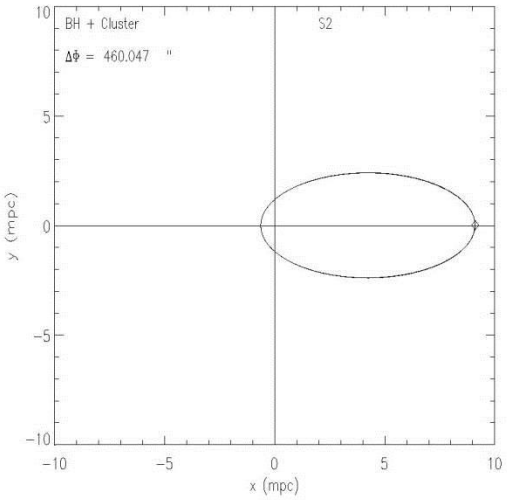
BH + Cluster
S2
Δϕ = 460.047 "
y (mpc)
x (mpc)

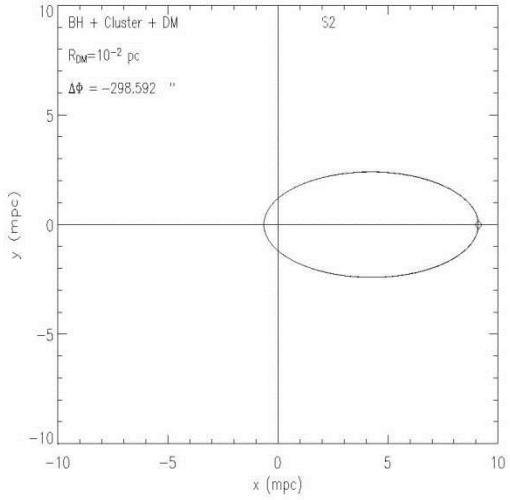
BH + Cluster + DM
S2
R_DM=10^-2 pc
Δϕ = -298.592 "
y (mpc)
x (mpc)

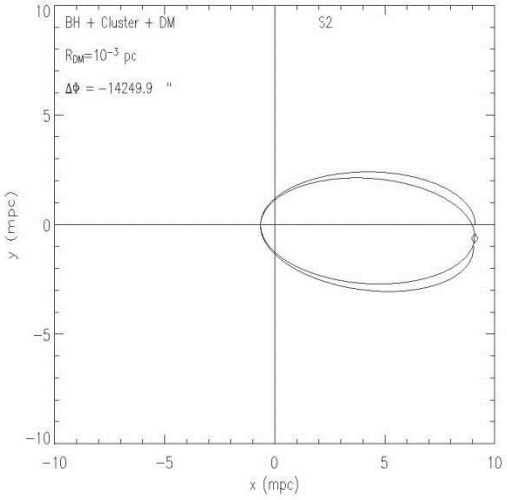
BH + Cluster + DM
S2
R_DM=10^-3 pc
Δϕ = -14249.9 "
y (mpc)
x (mpc)

Figure 31: PN-orbits for different mass configurations at the Galactic Center. The S2 star has been considered as a test particle and its apoastron shift is indicated in each panel as $\Delta\Phi$ (in arcsec). The top-left panel shows the central black hole contribution to the S2 shift that amounts to about 580 arcsec. The top-right panels shows the combined contribution of the black hole and the stellar cluster (taken following eq. 18) to the S2 apoastron shift. In the two bottom panels the contribution due to two different DM mass-density profiles is added (as derived in eq. 19). We assume that DM mass $M_{DM} \simeq 2 \times 10^5$ $M_\odot$.

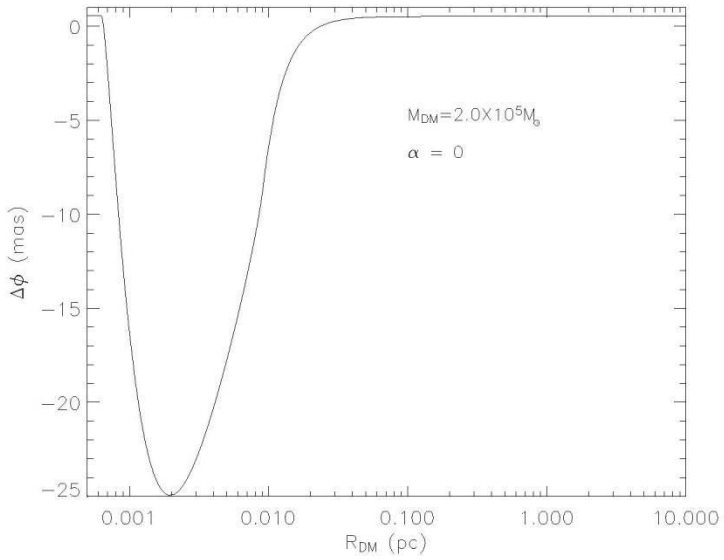

Figure 32: Apoastron shift as a function of the DM radius R_{DM} for $\alpha = 0$ and $M_{DM} \simeq 2 \times 10^5$ $M_\odot$. Taking into account present day precision for the apoastron shift measurements (about 10 mas) one can say that DM radii R_{DM} in the range $8 \times 10^{-4} - 10^{-2}$ pc are not acceptable.

D. Borka, P. Jovanovic, V. Borka Jovanovic and AFZ, PRD, **85**, 124004 (2012).

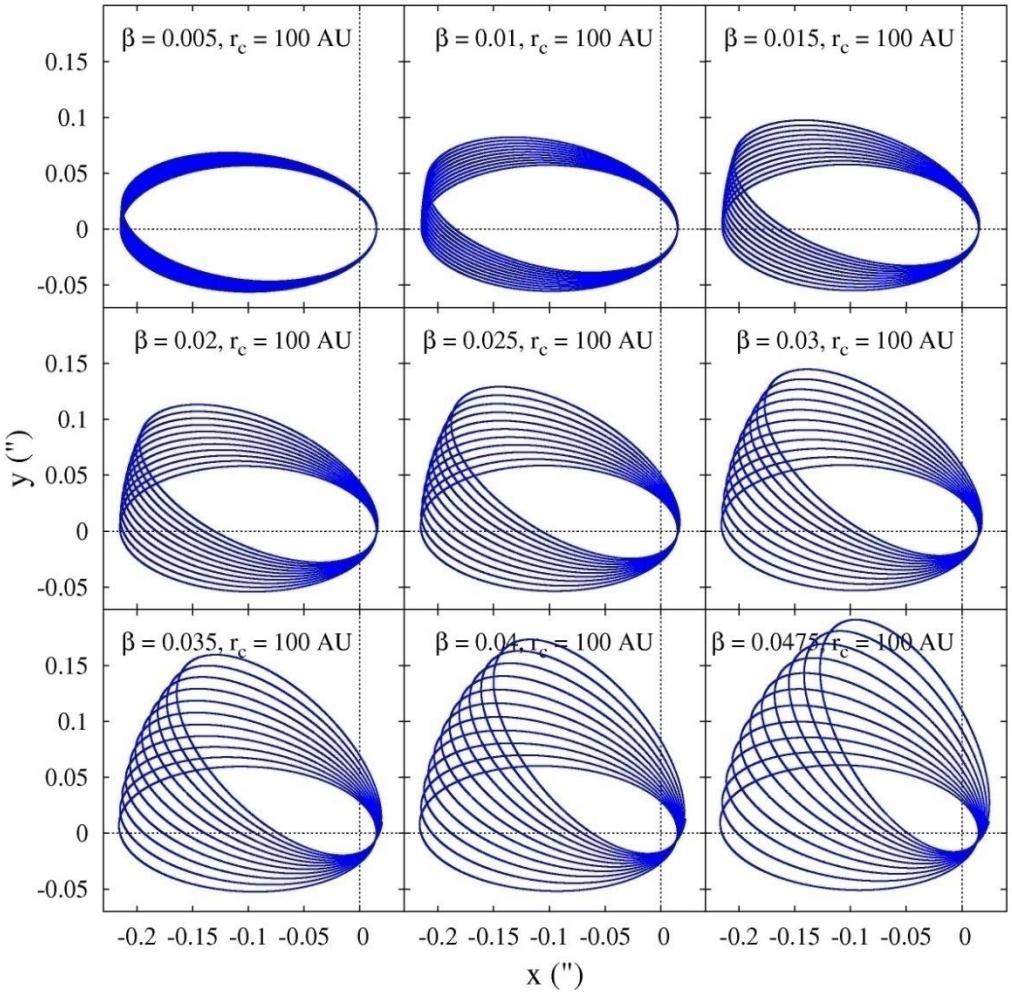

D. Borka, V. Borka Jovanovic, P. Jovanovic, AFZ

From an analysis of S2 orbit one can find signatures of Yukawa gravity (submitted)

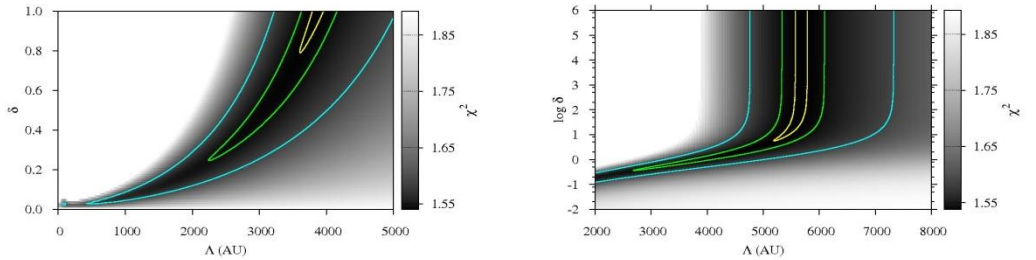

FIG. 7: **The maps of reduced χ^2 over the $\Lambda - \delta$ parameter space in case of NTT/VLT observations. The left panel corresponds to $\delta \in [0, 1]$, and the right panel to the extended range of $\delta \in [0.01, 10^6]$.** The shades of gray color represent the values of the reduced χ^2 which are less than the corresponding value in the case of Keplerian orbit, and three contours (from inner to outer) enclose the confidence regions in which the difference between the current and minimum reduced χ^2 is less than 0.0005, 0.005 and 0.05, respectively.

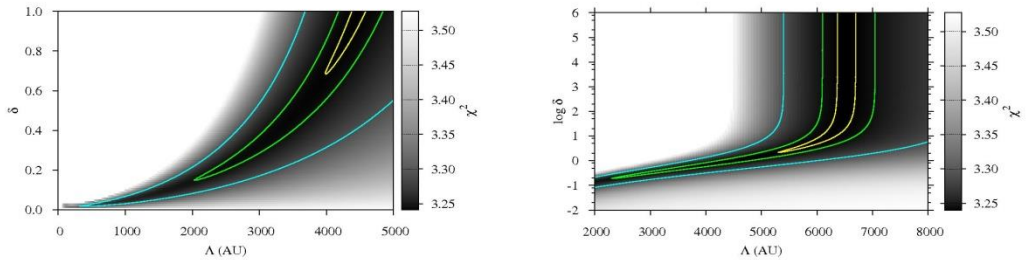

FIG. 8: **The same as in Fig. 7, but for the combined NTT/VLT+Keck observations.**

Yukawa gravity Λ which was varied from 10 to 10 000 AU. In the case of NTT/VLT observations the minimum of reduced χ^2 is 1.54 and is obtained for $\Lambda = 2.59 \times 10^3$ AU, while in the case of NTT/VLT+Keck combined data set the minimal value of 3.24 is obtained for $\Lambda = 3.03 \times 10^3$ AU. For both cases the reduced χ^2 for Keplerian orbits ($\delta = 0$) are 1.89 and 3.53, respectively, and thus significantly higher than the corresponding minima for $\delta = 1/3$. This means that Yukawa gravity describes observed data even better than Newtonian gravity and that $\delta = 1/3$ is valid value at galactic scales.

Figs. 7 and 8 present the maps of the reduced χ^2 over the $\Lambda - \delta$ parameter space for all simulated orbits of S2 star which give at least the same or better fits than the Keplerian orbits. These maps are obtained by the same fitting procedure as before. **The left panels of both figures correspond to $\delta \in [0, 1]$ and Λ[AU] $\in [10, 5000]$, and the right panels to the extended range of $\delta \in [0.01, 10^6]$ and Λ[AU] $\in [2000, 8000]$.** Three contours (from inner to outer) enclose the confidence regions in which the difference between the current and minimum reduced χ^2 is less than 0.0005, 0.005 and 0.05, respectively. **As it can be seen from Fig. 7, the most probable value for the scale parameter Λ, in the case of NTT/VLT observations of S2 star, is around 5000 - 6000 AU, while in the case of NTT/VLT+Keck combined data set (Fig. 8), the most probable value for Λ is around 6000 - 7000 AU. In both cases χ^2 asymptotically decreases as a function of δ, and hence, it is not possible to obtain reliable constrains on the universal constant δ of Yukawa gravity. Also, these two parameters δ and Λ are highly correlated in the range $(0 < \delta = +1/3 < 1)$. For $\delta > 2$ (the vertical strips) they are not correlated.**

As it could be also seen from left panels of Figs. 7 and 8, the values $\delta \approx 1/3$ result with very good fits for which the reduced χ^2 deviate from the minimal value for less than 0.005 (middle contours in both figures). The corresponding values for Λ range approximately from 2500 to 3000 AU. For $\delta = 1/3$ we obtained the following values: $\Lambda = 2590 \pm 5$ AU (NTT/VLT data) and $\Lambda = 3030 \pm 5$ AU (NTT/VLT+Keck combined data).

Although both observational sets indicate that the orbit of S2 star might be not a Keplerian one, the current astrometric limit is not sufficient to unambiguously confirm such a claim. However, the accuracy is constantly improving from around 10 mas during the first part of

- **Conclusions**

- VLBI systems in mm and sub-mm bands could detect mirages (“faces”) around black holes.
- Shapes of images give an important information about BH parameters
- Trajectories of bright stars or bright spots around massive BHs are very important tool for an evaluation of BH parameters
- Trajectories of bright stars or bright spots around massive BHs can be used to obtain constraints on alternative theories of gravity (f(R) theory, for instance)
- A significant tidal charge of the BH at GC is excluded by observations , but there signatures of extreme RN charge (perhaps non-electric one)

- **The main conclusion**

- Perhaps the BH model is not the best and final one, but it is working (alternative models have to explain the observational data as well to be adopted as realistic ones). A criticism has to be constructive.

- Thanks for your kind attention!

The Galaxy

Diàmeter: 25 kpc

Spiral galaxy with bar

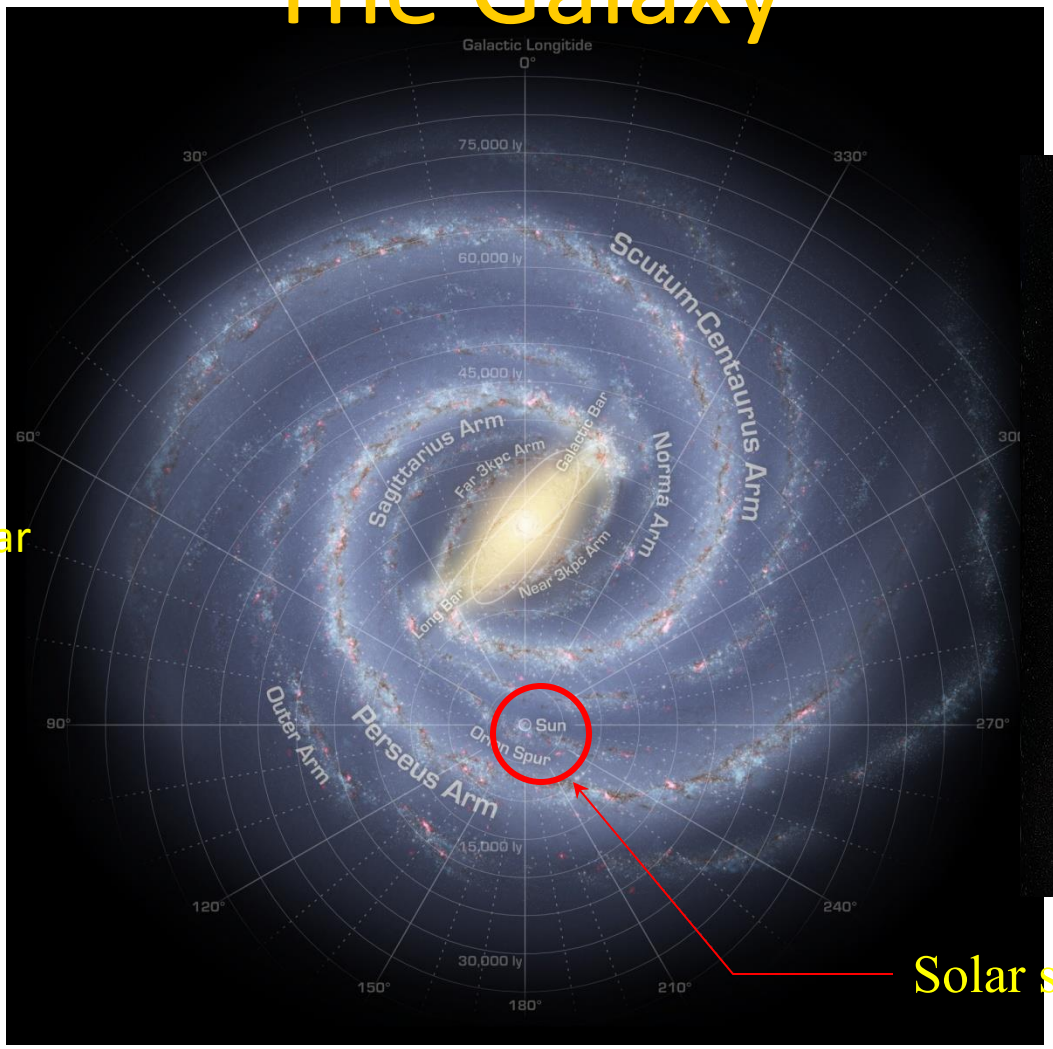

Solar system

Possible origin of flares

Flare: matter is heated on a (the innernmost stable) circular orbit (30 μas if J=0)

Flare period: period of the orbit

Fantastic tool to study general relativity in the strong field regime.

The *hot spot* will be used as a test particle to measure the space time around Sgr A*.

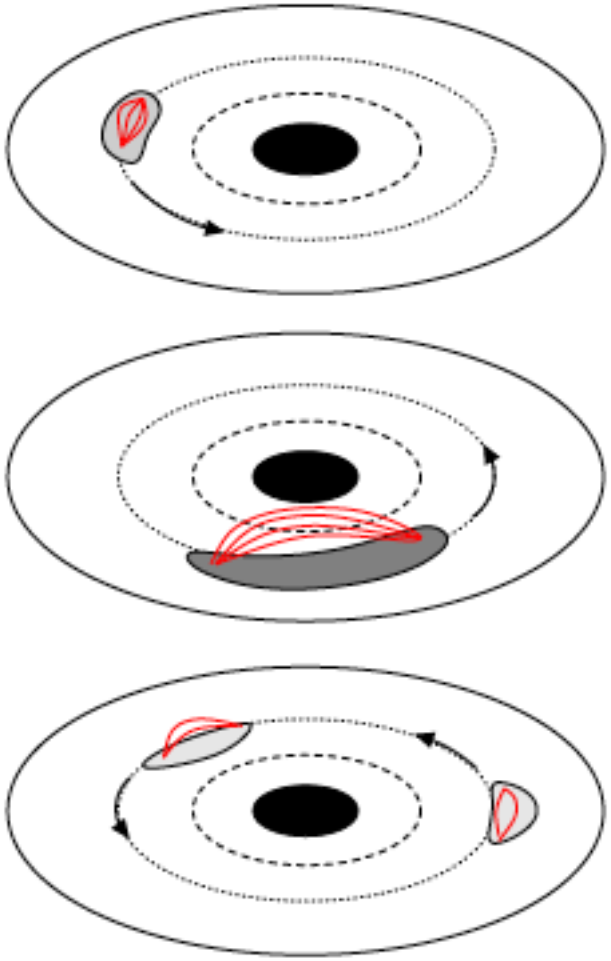

Eckart et al. A&A 500, 935 (2009)